



HAL
open science

Dynamic Image Quantization using Leaky Integrate-and-Fire Neurons

Effrosyni Doutsis, Lionel Fillatre, Marc Antonini, Panagiotis Tsakalides

► **To cite this version:**

Effrosyni Doutsis, Lionel Fillatre, Marc Antonini, Panagiotis Tsakalides. Dynamic Image Quantization using Leaky Integrate-and-Fire Neurons. 2019. hal-02351180v1

HAL Id: hal-02351180

<https://hal.science/hal-02351180v1>

Preprint submitted on 6 Nov 2019 (v1), last revised 22 Mar 2021 (v2)

HAL is a multi-disciplinary open access archive for the deposit and dissemination of scientific research documents, whether they are published or not. The documents may come from teaching and research institutions in France or abroad, or from public or private research centers.

L'archive ouverte pluridisciplinaire **HAL**, est destinée au dépôt et à la diffusion de documents scientifiques de niveau recherche, publiés ou non, émanant des établissements d'enseignement et de recherche français ou étrangers, des laboratoires publics ou privés.

Dynamic Quantization using Spike Generation Mechanisms

Effrosyni Doutsis, *Member, IEEE*, Lionel Fillatre, Marc Antonini, *Member, IEEE*,
Panagiotis Tsakalides, *Member, IEEE*,

Abstract—This paper introduces a neuro-inspired coding/decoding mechanism of a constant real value by using a Spike Generation Mechanism (SGM) and a combination of two Spike Interpretation Mechanisms (SIM). One of the most efficient and widely used SGMs to encode a real value is the Leaky-Integrate and Fire (LIF) model which produces a spike train. The duration of the spike train is bounded by a given time constraint. Seeking for a simple solution of how to interpret the spike train and to reconstruct the input value, we combine two different kinds of SIMs, the time-SIM and the rate-SIM. The time-SIM allows a high quality interpretation of the neural code and the rate-SIM allows a simple decoding mechanism by counting the spikes. The resulting coding/decoding process, called the Dual-SIM Quantizer (Dual-SIMQ), is a non-uniform quantizer. It is shown that it coincides with a uniform scalar quantizer under certain assumptions. Finally, it is also shown that the time constraint can be used to control automatically the reconstruction accuracy of this time-dependent quantizer.

Index Terms—Quantization, Leaky-Integrate and Fire Model, Spike Count, Uniform Scalar Quantizer.

I. INTRODUCTION

THEORETICAL neuroscience provides a qualitative basis for describing what is the nervous system, how does it work and which are the functions, the structure and the general principles by which it operates. Neuromathematical models have many different applications in computer vision, sensory-motor integration, neuromorphic hardware and artificial intelligence, among others.

We are interested in studying a novel coding/decoding architecture for signals, images and videos which is inspired by the neurons. In the literature, there are plenty of *Spike Generation Mechanisms (SGM)* which approximate the way the neurons transform a constant positive input stimulus I into a sequence of $N \in \mathbb{N}^+$ discrete events called a spike train. Each discrete event, namely a spike, is generated if the input intensity is stronger than a threshold θ , otherwise the neuron remains silent. The spikes are treated as identical stereotype events, because their shape does not seem to carry any information. Rather, it is the number of spikes and/or the spike arrival times which matter [1].

During the last decade, the neural spiking mechanisms have attracted the interest of the signal processing society because

they may reveal how to design power-efficient encoders and networks by encoding analog signals into spikes. Rank order coders [2], [3], time encoding machines [4], [5] and Asynchronous Pulse Sigma-Delta Modulators (APSDM) [6] are few of the latest architectures which use neural models in order to encode signals using spikes.

It is a general truth that neuroscientists are interested in exploiting SGMs but since the brain uses the code of spikes to learn, analyze, and take decisions instead of reproducing the input stimulus, the decoding process is out of their research scope. Nevertheless, the interpretation of the spike trains remains a highly important issue for many applications such as signal and image processing with constrained power and/or neuromorphic devices. Thus, it is highly important to find out the best *Spike Interpretation Mechanism (SIM)* which allows us to use the code of spikes and reconstruct the highest quality input signal (Fig. 1).

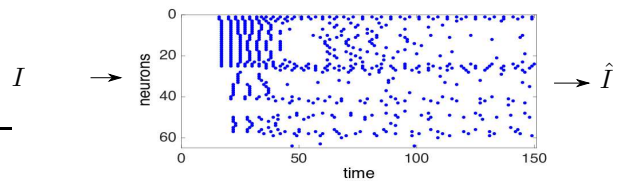


Fig. 1: General framework of the proposed architecture. A group of 60 neurons receives an input stimulus I which is flashed for 150 ms. The neurons generate some spike trains, after a short period of silence, which are used to reconstruct an approximation \hat{I} . The delayed response of the neurons is justified by the location of ganglion cells. In addition, the visual stimulus is first captured and transformed, by the time-varying receptive field of the former retina cells, into a low-energy signal that turns into high-energy as time increases. Thus, the neurons need more time to be excited [7].

The main contributions of the paper are the following. First, the paper introduces a novel quantizer, namely the *Dual-SIM Quantizer (Dual-SIMQ)*, which is based on two complementary aspects of SIM: i) the input value is converted into a sequence of spikes by using a time-encoding and ii) it is reconstructed by using a rate-decoding which counts the spikes. It is shown that the combination of time-coding and rate-decoding leads to a natural quantization of the input value. Second, the maximum number of spikes is controlled by a given observation duration $T > 0$. The duration T is interpreted as the maximum time period which is allowed

E. Doutsis was with Université Côte d'Azur, I3S, CNRS in the beginning of this work. She is now with Foundation for Research and Technology-Hellas (FORTH) (e-mail: edoutsis@ics.forth.gr).

L. Fillatre and M. Antonini are with Université Côte d'Azur, CNRS, I3S, France (e-mail: lionel.fillatre@i3s.unice.fr; am@i3s.unice.fr).

P. Tsakalides is with University of Crete and Foundation for Research and Technology-Hellas (FORTH) (e-mail: tsakalid@ics.forth.gr).

to encode and decode the spike train. The behavior of the whole quantizer is dependent of this parameter T . Hence, this time constraint generates a dynamic quantizer whose behavior evolves in time. The dynamic properties of the Dual-SIMQ give rise to a ground-breaking compression system that permits a time-dependent quality refinement of the reconstructed signal. This is a great breakthrough compared to the conventional quantizers which process the input stimulus for a single time without taking advantage of the observation duration. The impact of such a behavior might become apparent if we consider videos. It is shown that this novel neuro-inspired mechanism is a non-uniform quantizer which can coincide with a Uniform Scalar Quantizer (USQ) by choosing adequately some of its parameters.

Section II describes the principle of the neuro-inspired quantization based on spike trains. Section III is an overview of the spike generation and interpretation mechanisms, focusing especially on the Leaky Integrate-and-Fire (LIF) model which is the most well known model. Section IV presents our main contribution. It shows how to combine the rate-SIM and time-SIM to derive the Dual-SIMQ. Numerical results on both simulated data and real data are presented in Section V. A concise discussion and the conclusion of this work are drawn in section VI.

II. PRINCIPLE OF NEURO-INSPIRED QUANTIZATION

This section briefly recalls the main concepts in quantization and rate-distortion theory and how they are related to the neuro-inspired quantization.

A. Basics of Quantization

Let I be a real random variable with the probability density function (pdf) $p(I)$ and let the representation of I be denoted as \hat{I} . If we are given r bits to represent I , the value \hat{I} can take on 2^r values. The general problem of quantization is to find the optimum set of values for \hat{I} , called the code points $\hat{I}_1, \hat{I}_2, \dots$ and the regions S_1, S_2, \dots , that are associated with each code point.

According to quantization theory [8], a 2^r -rate distortion code consists of an encoding function,

$$f : \mathbb{R} \rightarrow \mathcal{C}, \quad (1)$$

where \mathcal{C} is a subset with 2^r elements of the set of all integers \mathbb{Z} and a decoding function

$$g : \mathcal{C} \rightarrow \mathbb{R}. \quad (2)$$

The encoding function defines a partition $\{S_1, \dots, S_{2^r}\}$ of \mathbb{R} such that $S_i \cap S_j = \emptyset$ for all $i \neq j$ and $\cup_{m=1}^{2^r} S_m = \mathbb{R}$. The interval S_m is called the m -th quantization region and it is defined such that $f(I)$ is constant for all $I \in S_m$ and $g(f(I)) = \hat{I}_m$ for all $I \in S_m$.

The quantization can be uniform or non-uniform [9], [10]. A uniform quantizer is recommended when the input source is either uniformly or non-uniformly distributed but in the latter case it is mandatory that the quantizer is followed by an entropy coder where the statistics of the input source are taken into consideration. Otherwise, it is better to calculate

some non-uniform quantization regions such that finer regions are associated to more likely values. Several non-uniform approaches are possible: i) use a uniform quantizer anyway (with an optimal choice of the quantization step q); ii) use a non-uniform quantizer (by choosing the quantization regions and values); iii) transform the input value into one that looks uniform and use a uniform quantizer (this is called the compander/expender approach). This paper does not make any assumption on the probability distribution of the input value.

Most uniform quantizers for signed input value can be classified as being of one of two types: mid-rise and mid-tread. A typical mid-rise uniform scalar quantizer with a quantization step size $q > 0$ can be expressed as

$$Q_q(x) = q \cdot \left(\left\lfloor \frac{x}{q} \right\rfloor + \frac{1}{2} \right), \quad (3)$$

where the notation $\lfloor x \rfloor$ corresponds to the greatest integer less than or equal to x . For simplicity, it is assumed that $\mathcal{C} = \mathbb{Z}$ is not finite. The encoding function $f(x)$ is given by

$$f(x) = \left\lfloor \frac{x}{q} \right\rfloor \quad (4)$$

and the decoding function is

$$g(k) = q \cdot \left(k + \frac{1}{2} \right), \quad \forall k \in \mathcal{C}. \quad (5)$$

The definition of the mid-tread uniform scalar quantizer with deadzone $\lambda > 0$ is given by:

$$Q_{q,\lambda}(x) = \text{sgn}(x) \max \left(0, \left\lfloor \frac{|x| - \lambda/2}{q} + 1 \right\rfloor \right) \times q, \quad (6)$$

where $\text{sgn}(I)$ denotes the sign of I : $\text{sgn}(I) = 1$ if $I > 0$, $\text{sgn}(I) = -1$ if $I < 0$ and $\text{sgn}(0) = 0$. The zero output of the quantizer is the interval $[-\frac{\lambda}{2}, \frac{\lambda}{2}]$ called the deadzone. The standard mid-tread quantizer corresponds to $\lambda = q$. The encoding function is

$$f(x) = \text{sgn}(x) \cdot \max \left(0, \left\lfloor \frac{|x| - \lambda/2}{q} + 1 \right\rfloor \right), \quad (7)$$

and the decoding function is

$$g(k) = \text{sgn}(k) \cdot \left(\frac{\lambda}{2} + q \cdot \left(|k| - \frac{1}{2} \right) \right), \quad \forall k \in \mathcal{C}. \quad (8)$$

It has been proven that given a certain statistical distribution of the signal it is possible to compute the best partition that minimizes the power of noise using the Lloyd quantizer which is explicitly described in [11].

B. Neuro-Inspired Quantization

The neuro-inspired quantizer proposed in this paper encodes the input value as a spike train and it exploits this spike train to estimate \hat{I} . More formally, it is assumed that the input value I takes the form of a constant signal

$$I(t) = I \mathbf{1}_{[0 \leq t \leq T]}(t), \quad (9)$$

for a given duration $T > 0$ where $\mathbf{1}$ is the indicator function which equals 1 if $0 \leq t \leq T$, and 0 otherwise. Without any loss of generality, it is assumed that $I \geq 0$. It will be mathematically defined later on (see section IV-B), that if I is

real, the sign of I will be coded separately with a dedicated single bit. The encoding function is then a function $f(I)$ which transforms the signal $I(t)$ into a spike train

$$f(I) = \{t^1(I), t^2(I), \dots, t^{N(I)}(I)\} = \{t^1, t^2, \dots, t^N\}$$

of $N = N(I)$ increasing positive time values $t^j = t^j(I)$ depending on I . The decoding function $g(\cdot)$ transforms the spike train $f(I)$ in an estimated real value $\hat{I} = g(f(I))$. In the rest of the paper, the symbol I is omitted in the spike times t^j and N in order to simplify the notations. The duration T acts as a parameter to control the number N of spikes.

C. Basics of Rate Distortion Theory

The distortion of a quantizer can be measured by the Mean Squared Error (MSE):

$$D = \text{MSE}(I, \hat{I}) = \sum_{m=1}^L \int_{S_m} (I - \hat{I}_m)^2 p(I) dI, \quad (10)$$

where L is the number of the quantization layers. In the case of a high resolution uniform scalar quantizer, when q is small (or equivalently L sufficiently large), assuming that the pdf $p(I)$ is smooth enough, it is shown in [9] that

$$D \approx \frac{q^2}{12}. \quad (11)$$

The rate is given by the entropy of the codewords:

$$r = - \sum_{m=1}^L p_m \log_2 p_m, \quad (12)$$

where $p_m = \int_{S_m} p(I) dI$ is the probability of the quantization interval S_m . We also get from [12] that:

$$r \approx H(I) - \log_2 q, \quad (13)$$

where $H(I) = \int_{-\infty}^{+\infty} p(I) \log_2 p(I) dI$ is the Shannon entropy. Finally, we obtain the famous rate-distortion approximation

$$D = D(r) \approx \frac{1}{12} 2^{2H(I)} 2^{-2r}, \quad (14)$$

which gives the optimum value of D for a given rate r in the case of a high resolution uniform quantizer.

III. SPIKE GENERATION AND INTERPRETATION

This section describes usual mechanisms to transform a signal into a spike train and to recover it from the spike train.

A. Spike Generation Mechanism (SGM)

In the literature, there are several models which approximate the neural activation. Hodgkin and Huxley [13] reproduced the neural activity with high accuracy deriving a set of four nonlinear differential equations which approximate the neural behavior with a lot of details at the level of ion channels. However, these equations are difficult to manipulate. A possible reduction of these equations leads to either a system of two-dimensions [14]–[17] or the Spike Response Model (SRM) [1], [18], [19]. On the one hand, the advantage of the

two-dimension simplification is the plane analysis of the neural behavior. On the other hand, based on the SRM, it is proven in [18] that the Hodgkin-Huxley equations can be approximated by the simpler Leaky Integrate-and-Fire (LIF) model [1].

The well-known LIF model is simple [1]. It approximates the neuronal encoding process by a first order differential equation derived from a resistor-capacitor circuit:

$$I(t) = \frac{u(t)}{R} + C \frac{du}{dt}(t), \quad (15)$$

where $I(t)$ is the input signal, C is the capacitance, R is the resistance and $u(t)$ is the voltage across the resistor. The voltage $u(t)$ models the membrane potential of a neuron. It is assumed that $u(t = t^{(k)}) = 0$ mV after the emission of a spike at time $t^{(k)}$, $k \geq 1$, with the convention that $t^{(0)} = 0$ ms.

The solution $u_k(t)$ of the differential equation (15) for the constant signal $I(t)$ in (9) after the emission of the k -th spike at time $t^{(k)}$ is given by:

$$u_k(t) = RI \left[1 - \exp\left(-\frac{t - t^{(k)}}{\tau}\right) \right], \quad \forall t \geq t^{(k)}, \quad (16)$$

where $\tau = RC$ is the time constant. The neuron spikes when $u_k(t)$ crosses the threshold $\theta > 0$. The moment $t^{(k+1)}$ the neuron spikes is called the $(k+1)$ -th firing time and it satisfies

$$u_k(t^{(k+1)}) = \theta. \quad (17)$$

It follows that

$$t^{(k+1)} = \begin{cases} +\infty, & \text{if } RI \leq \theta, \\ t^{(k)} - \tau \ln \left[1 - \frac{\theta}{RI} \right], & \text{if } RI > \theta. \end{cases} \quad (18)$$

Just after the emission of the $(k+1)$ -th spike at time $t^{(k+1)}$, the potential is reset to zero, i.e., $u_{k+1}(t^{(k+1)}) = 0$, and the integration of the potential starts all over again for $t > t^{(k+1)}$ until the next spike emission. The asymptotic value RI determines the generation of the spikes: if $RI \leq \theta$, there is no spike, otherwise, a spike is emitted. This paper does not consider any absolute refractory period [1] after the spike emission.

B. Spike Interpretation Mechanism (SIM)

Due to the fact that spikes are characterized as stereotype events, the information which is carried on a spike train is either the number of spikes or the time each spike arrives. This subsection is dedicated to the analysis and comparison of the most widely used Spike Interpretation Mechanisms (SIMs), the *rate-SIM* and the *time-SIM*.

1) *Rate-SIM*: The spiking activity of a neuron over time is usually represented by a graph called the raster plot as shown in Fig. 1. Under the assumption that the neurons are independent, it has been proven that for a given input $I(t)$ the firing rate is a stochastic process which causes irregular interspike intervals reflecting a random process [20], [21]. Then, the instantaneous spike rate (mean firing rate) can be obtained either by averaging the spikes of an individual neuron (*spike count*), or by averaging the firing rate over multiple repetitions of the same experiment (*spike density*) [1]. The spike density can be interpreted as a time-dependent mean firing rate. The rate-SIM is certainly the most traditional

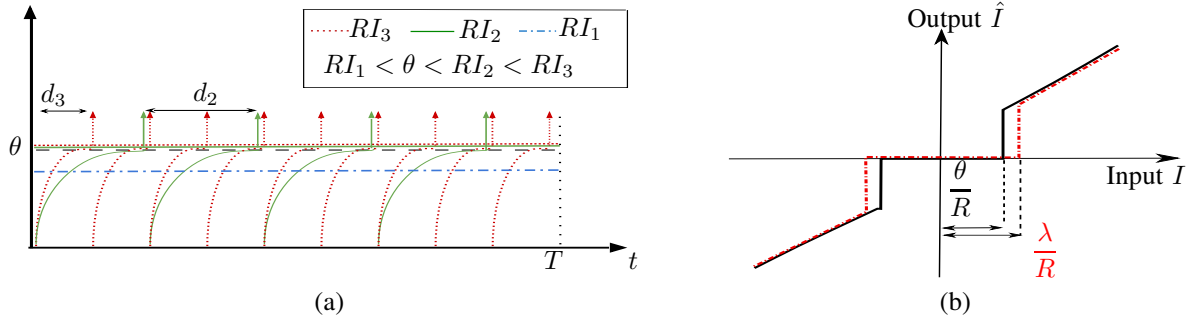


Fig. 2: (a) LIF model for the observation window duration T and the threshold θ . If the intensity I satisfies $RI > \theta$, the neuron spikes (case $I \in \{I_2, I_3\}$), otherwise it remains silent (case $I = I_1$). (b) Black solid line: the Perfect-LIF enables the reconstruction of values $I > \theta/R$. Red dash-dotted line: the Perfect-LIF enables the reconstruction of values $I \geq \lambda/R$ due to the temporal constraint T .

approach but it is so simplistic that it seems to be rather an intuitive than a reliable method. Indeed, the rate-SIM neglects all the information hidden in the time each spike arrives.

2) *Time-SIM*: An alternative strategy is to interpret a code of spikes by exploiting the time a neuron emits its spikes. Generally, the time-to-first-spike is a time-SIM which assumes that the neuron which fires shortly after the onset of the stimulus is more sensitive to the input comparing to other neurons which are activated somewhat later [22]–[26]. Another famous time-SIM code is the Rank-Order-Coder (ROC) which identifies the spike train of a neuron by ranking the arrival of the first spike. A strong stimulus corresponds to a fast arrival of a spike (low rank) while a weak stimulus results in a late or no response (high rank) [2], [22], [27], [28]. Finally, the LIF can also be considered as a time-SIM as discussed hereafter.

According to Subsection III-A, the LIF encodes the input stimulus into the spike train $\{t^{(1)}, \dots, t^{(N)}\}$. From the definition of the arrival times $t^{(k+1)}$ in (18), it follows that the delay $d = d(I)$ between two spikes arrivals is constant because I is constant, i.e., $d = t^{(k+1)} - t^{(k)}$ for any k , and satisfies

$$d(I) = \begin{cases} +\infty, & \text{if } RI < \theta, \\ h(I) = -\tau \ln \left[1 - \frac{\theta}{RI} \right], & \text{if } RI > \theta. \end{cases} \quad (19)$$

The stronger the input signal is, the smaller the delay between spikes. On the contrary, a weak input signal corresponds to a larger delay. Fig. 2(a) illustrates the LIF model for three different temporally constant inputs $I_1 < I_2 < I_3$ and a threshold θ . Based on (19), the intensities I_2 and I_3 are able to spike with delays $d_3 < d_2$. The third intensity I_1 remains silent because $RI_1 < \theta$ and its spiking delay turns to infinity.

Let us denote $h^{-1}(d)$ the inverse function of $h(I)$ given by

$$h^{-1}(d) = \frac{\theta}{R \left(1 - \exp \left(-\frac{d}{\tau} \right) \right)}, \quad \text{for } d \neq 0. \quad (20)$$

If the delay d , finite or infinite, was perfectly known, the reconstructed value would be \hat{I} :

$$\hat{I} = \begin{cases} 0, & \text{if } d > T, \\ h^{-1}(d), & \text{if } d \leq T. \end{cases} \quad (21)$$

When d is larger than the observation duration T , the receiver

does not receive any spike. Hence, any arbitrary value of \hat{I} is acceptable; the zero value is a reasonable choice. In addition, there is no error of reconstruction when the delay is smaller than T . Based on the analysis above, the substitution of the delay d with the observation window T in (20) results in a new threshold λ associated to the reconstruction error

$$\lambda = R h^{-1}(T) = \theta \left(1 - \exp \left(-\frac{T}{\tau} \right) \right)^{-1}. \quad (22)$$

Therefore, according to the aforementioned example where the delay is perfectly known, if $RI > \lambda$ there will be no reconstruction error. It can be noted that $\lambda > \theta$ (since $T > 0$ and $\tau > 0$) and λ converges to θ as T becomes arbitrarily large.

The characteristic function of such a “perfect” coding/decoding system, called the *Perfect-LIF* in [29], is a thresholding function as shown in Fig. 2(b). The solid line shows the perfect-LIF without any time constraint (infinite observation time) and the dashed-dotted line shows the perfect-LIF with the bounded observation time T . The temporal constraint T implies that all the input value I such that $\theta < RI \leq \lambda$ can not be recovered by the time-constrained perfect-LIF. Obviously, as discussed in [30], the transmission of the exact value of the delay d is very expensive regarding the number of coding bits. To decrease the binary rate of the perfect-LIF, this paper proposes to combine the spike counter rate-SIM and the delay coder time-SIM mechanisms resulting in the Dual-SIMQ. Using the rate-SIM decoder allows us to have a simple decoding mechanism which works for any T .

IV. DUAL-SIM QUANTIZER

This section is dedicated to the analysis of our novel Dual-SIMQ which was first briefly introduced in [30].

A. Dual-SIMQ Coder/Decoder

The first step of the Dual-SIMQ encoder consists in encoding the input value I as a spike train by using the LIF encoder (18). When the input signal is constant, since the interspike delay (19) is constant, we propose to count the

spikes instead of coding the interspike delay. The theoretical number of spikes over the time interval $[0, T]$ is:

$$N = N(I) = \begin{cases} 0, & \text{if } RI \leq \lambda, \\ \lfloor \frac{T}{d(I)} \rfloor, & \text{if } RI > \lambda. \end{cases} \quad (23)$$

If one counts the number of spikes N for a fixed observation window T , the delay $d = d(I)$ can be easily estimated by

$$\hat{d} = \begin{cases} \infty, & \text{if } N = 0, \\ \frac{T}{N} & \text{if } N > 0. \end{cases} \quad (24)$$

Fig. 3 illustrates how the Dual-SIMQ counts the number of spikes with respect to the input intensity I . For any input intensity I such that $RI < \lambda$, there will be no spikes emitted ($N = 0$) because $\hat{d} > T$. Consequently, all the input values which belong to interval

$$S_0 = \{I > 0 : RI < \lambda\} = [0, h^{-1}(T)) \quad (25)$$

will be recovered by the single output intensity $\hat{I}_0 = 0$. Based on the above equation, it is obvious that the length ℓ_0 of the interval S_0 is $\ell_0 = \lambda/R$. Let us now suppose that only one spike arrives for the input signal I , i.e., $N = 1$. According to (23), all the input intensities I which have caused the generation of a single spike belong to

$$S_1 = \left\{ I > 0 : \frac{T}{2} < d(I) \leq T \right\}. \quad (26)$$

According to the quantization theory [9], assuming that the pdf, $p(I)$, is uniform over S_1 , it is well known that the MSE error is minimized when the quantization interval is represented by its center. Hence, we choose to reconstruct any value I associated to S_1 as

$$\hat{I}_1 = \frac{1}{2} \left(h^{-1} \left(\frac{T}{2} \right) + h^{-1}(T) \right). \quad (27)$$

With the same reasoning, let us define S_k as the quantization region associated to the input value I which has generated exactly k spikes for any $k \geq 1$, i.e.,

$$S_k = \left\{ I > 0 : \frac{T}{k+1} < d(I) \leq \frac{T}{k} \right\}. \quad (28)$$

The length ℓ_k of an interval S_k for $k \geq 1$ is given by

$$\ell_k = h^{-1} \left(\frac{T}{k+1} \right) - h^{-1} \left(\frac{T}{k} \right). \quad (29)$$

A value $I \in S_k$ is reconstructed by the interval's centroid value

$$\hat{I}_k = \frac{1}{2} \left(h^{-1} \left(\frac{T}{k+1} \right) + h^{-1} \left(\frac{T}{k} \right) \right). \quad (30)$$

B. Dealing with real values

In signal processing, it is very common that an input source has to be first transformed before the quantization. The transformation enables to concentrate most of the signal information in few low frequency components. However, after the transformation, most of the times, occur negative values,

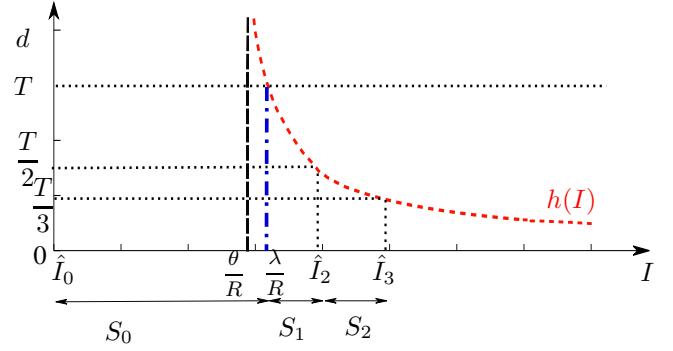


Fig. 3: The input values I is arranged in quantization regions S_k depending on the number k of emitted spikes.

so here we describe how the proposed Dual-SIMQ deals with negative inputs.

Suppose that the input value I corresponds to one of the pixel values of an image. We have decided to assign 1-bit per pixel to encode the sign of each input intensity as following

$$\text{sgn}(I) = \begin{cases} 1, & \text{if } I \geq 0, \\ -1, & \text{otherwise.} \end{cases} \quad (31)$$

Thus, the Dual-SIMQ coder receives as an input the absolute value of each input intensity $|I|$ and computes the number of the emitted spikes k within the observation window T . Then, the decoder receives the sign information, $\text{sgn}(I)$, and the number of spikes k which are associated to the quantization interval S_k represented by the centroid value $|\hat{I}|$. Finally, the output of the decoder is given by $\tilde{I} = \text{sgn}(I)|\hat{I}|$ and the reconstructed values belong to the set

$$\tilde{I} \in \{ \tilde{I}_0, \tilde{I}_1, \dots, \tilde{I}_k, \dots \}. \quad (32)$$

C. Dynamic Properties of the Dual-SIM Quantization

As explained in the previous sections, the performance of the Dual-SIMQ is mainly driven by the threshold parameter θ . Figure 4(a) shows for a normal distribution input that when the threshold value increases, the Dual-SIMQ generates a lot of distortion. This is also obvious if one plots the characteristic function of the Dual-SIMQ (see Fig. 4 (b)) where the length ℓ of the quantization steps are wider as theta increases. However besides θ , there are other parameters that also influence the Dual-SIMQ response such as the observation window T and the resistance R .

1) *Time-Dependent Dual-SIMQ*: The “dynamic” behavior of the Dual-SIMQ is one of its most important properties associated with the fact that the number of spikes depends on the length of the observation window T . According to (23), the longer the input signal is flashed, the more the spikes that correspond to this input intensity. On the other hand, if the observation window is too small, the number of spikes will fail to precisely describe the input signal.

As depicted in Fig. 4(c), for a normal distribution input, while increasing the observation window T , the quality of the reconstructed signal substantially improves. It is remarkable that when time is too short ($T < 20$ ms) the Dual-SIMQ is not able to perceive any information regarding the input

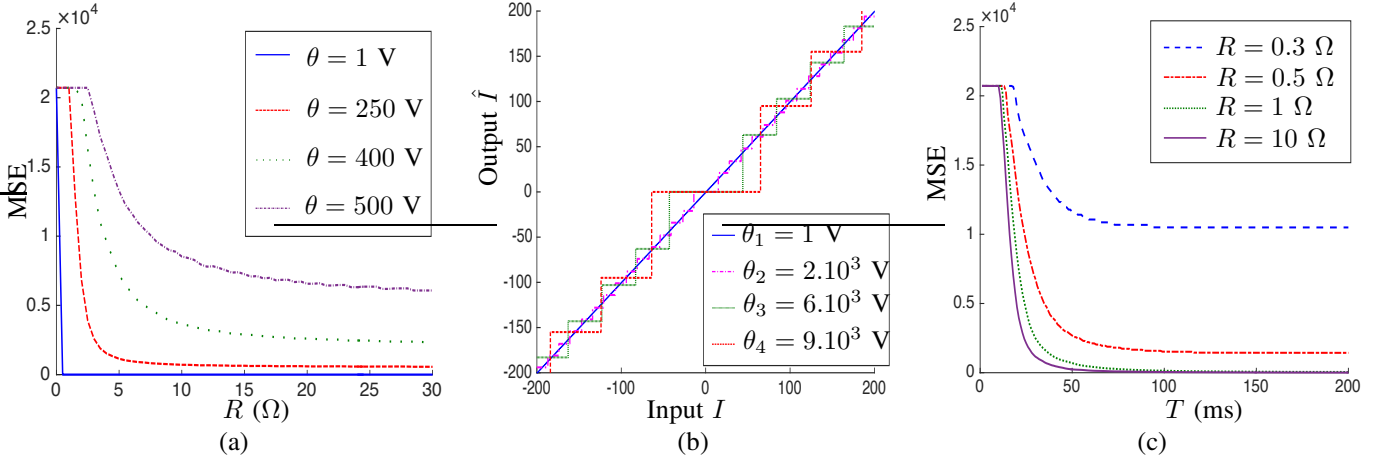


Fig. 4: (a) Impact of the threshold θ on the performance of the Dual-SIMQ; the distortion increases with theta (set of parameters: $C = 50$ F, $T = 200$ ms). (b) Dual-SIMQ characteristic function for different θ values (parameters: $T = 150$ ms, $R = 1000$ Ω , $C = 1$ F). (c) Impact of the size of the observation window T on the performance of the Dual-SIMQ. The reconstruction quality improves when the size of the observation window increases (set of parameters: $C = 50$ F, $\theta = 50$ V).

signal. This is a natural coincidence due to the neuroscience models which are embedded in the Dual-SIMQ. This time could be intuitively explained as the propagation time of the visual stimulus to the spiking neurons. In addition, it is obvious that at a given time ($T \approx 100$ ms) the reconstruction quality vanishes into an asymptotic value.

2) *Resistance-Dependent Dual-SIMQ*: It has been shown in [30] that the Dual-SIMQ can be approximated by a USQ for very large values of R . In this work, we extend this proof and we show that R determines the Dual-SIMQ response that varies from *uniform* to *non-uniform*.

Proposition 1. *Let us assume that the input value I has generated exactly k spikes for any $k \geq 1$ while the value of R is arbitrarily large. Then, the Dual-SIMQ is a uniform quantizer where the length ℓ_k of each quantization interval is constant for all k*

$$\ell_k = \frac{\theta C}{T} + o\left(\frac{1}{R}\right), \quad \forall k, \quad (33)$$

where the notation $o(\cdot)$ is the little- o notation, recalled in (44), which is used to express the asymptotic behavior of a function. Then, the number of the generated spikes is

$$N = N(I) = \left\lfloor \frac{T}{\theta C} I \right\rfloor. \quad (34)$$

Proof. Using the Taylor series it follows that, for $k \geq 1$,

$$h^{-1}\left(\frac{T}{k}\right) = \frac{\theta C}{T} k + \frac{\theta}{2R} + \frac{\theta T}{12 R^2 C k} + o\left(\frac{1}{R^2}\right). \quad (35)$$

Combining (29) and (35) yields (33). Furthermore, we get

$$\frac{\lambda}{R} = h^{-1}(T) = \frac{\theta C}{T} + \frac{\theta}{2R} + \frac{\theta T}{12 R^2 C} + o\left(\frac{1}{R^2}\right).$$

Finally, a short calculation based on the Taylor series of the logarithm shows that

$$d(I) = h(I) = \frac{\theta C}{I} + \frac{C\theta^2}{2RI^2} + o\left(\frac{1}{R}\right). \quad (36)$$

Incorporating (36) in (23) yields (34). \square

Proposition 1 shows that the Dual-SIMQ coincides with a USQ, $Q_{q=\ell_\infty, \lambda=2\ell_\infty}(x)$, as R becomes arbitrarily large, with a quantization step $q = \ell_\infty$. This confirms that a large T yields an accurate quantization. On the opposite, a large value of θ or C decreases the accuracy of the quantizer.

Proposition 2. *Let us now assume that R is small, then the Dual-SIMQ is a non-uniform quantizer. The length of each quantization interval depends on the number of spikes k . When k increases, the length ℓ_k converges to an asymptotic value*

$$\ell_k = \frac{\theta C}{T}, \quad k \rightarrow \infty. \quad (37)$$

Proof. See the proof in the Appendix A. \square

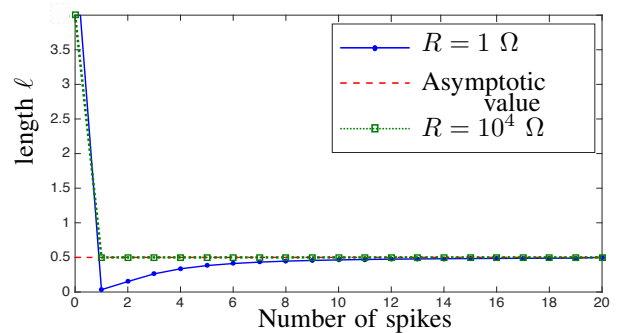


Fig. 5: This figure illustrates the performance of the Dual-SIMQ as a non-uniform quantizer when the value of R is small and as a uniform quantizer when the value of R is arbitrarily large (set of parameters: $\theta = 5$ V, $C = 10$ F and $T = 100$ ms).

Figure 5 illustrates how the value of R affects the length ℓ of the quantization intervals in function of the number of spikes. When R is small and $k \geq 1$, the length of the quantization interval is a strictly increasing function which is

upper-bounded by ℓ_0 . However, when R is large, the Dual-SIMQ becomes completely uniform. As we show later on, when the Dual-SIMQ is applied to a normal distribution signal, it is expected to better encode the low than the high intensities when R is small. On the contrary, whatever the intensity is, if R is high it will behave towards a uniform manner. The interpretation of the above behavior will be more evident in section V.

V. NUMERICAL RESULTS

The proposed neuro-inspired Dual-SIMQ is evaluated in terms of the rate-distortion trade-off on both simulated and real data.

A. Experiments with Simulated Data

In this section, we aim to study the validity of the rate-distortion theory which is determined by the comparison of the rate-distortion approximation and the performance of the Dual-SIMQ when the distribution of the input signal is normal. It has been proven in Section IV-C, that the Dual-SIMQ is a dynamic quantizer that performs either as a uniform or as a non-uniform transducer. The distortion approximation (11) is only related to an asymptotic behavior thus, the comparison is considered against the uniform Dual-SIMQ. If the constant length of the quantization intervals ℓ_k (37) takes the place of the quantization step q in (11), it is trivial to visualize that the distortion approximation perfectly overfits the behavior of the Dual-SIMQ.

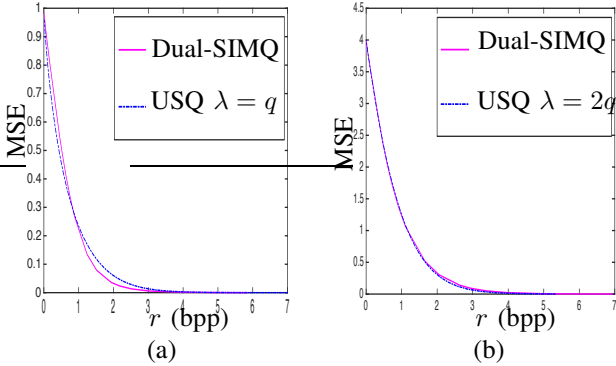


Fig. 6: Comparison of the asymptotic performance of the Dual-SIMQ with the USQ for inputs following (a) the Laplacian distribution and (b) the Gaussian distribution (set of parameters: $C = 1$ F, $R = 10^8$ Ω , $\theta \in [5, 500]$ V and $T = 150$ ms).

Fig. 6 compares the performance of the Dual-SIMQ and the USQ for input samples following Laplacian and Gaussian distributions. We have chosen these inputs because according to [12] for a USQ there is an optimal relationship between the quantization step q and the deadzone λ ; for Laplacian distributions the deadzone equals $\lambda = q$ and for Gaussian distributions $\lambda = 2q$. Proposition 1 has shown that the performance of the Dual-SIMQ is asymptotically equivalent to the optimal USQ.

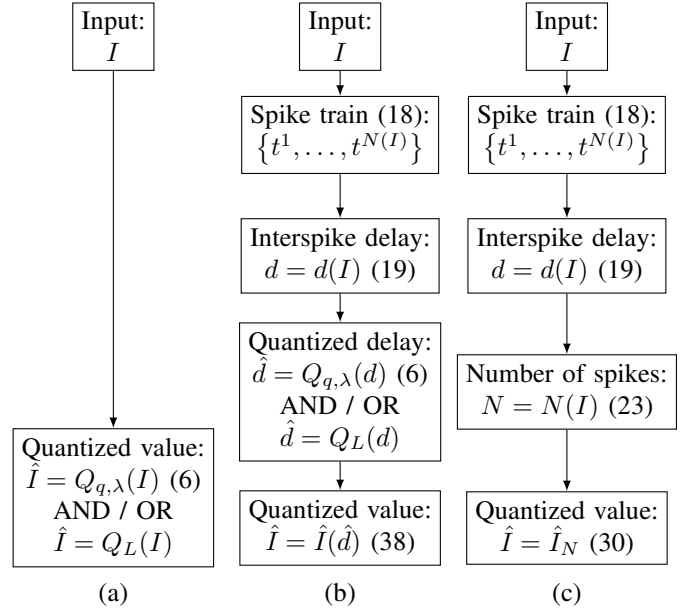


Fig. 7: Three kinds of quantization: (a) USQ $Q_{q,\lambda}$ or Lloyd Quantizer Q_L applied to I , (b) USQ $Q_{q,\lambda}$ or Lloyd Quantizer Q_L applied to delays $d(I)$, and (c) Dual-SIMQ.

B. Dual-SIMQ vs USQ on Real Data

It is proven in Section IV, that by tuning some of the Dual-SIMQ parameters its behavior might be uniform or non-uniform. For this reason, we have decided to contrast Dual-SIMQ with uniform and non-uniform state-of-the-art quantizers. Figure 7 illustrates the schema of every quantizer that participates to this comparison. The first quantization is a USQ or the Lloyd quantizer applied directly to the input value I (see Fig. 7 (a)). The second type of quantization is composed of three steps: i) the input value I is transformed in a spike train with a constant interspike delay $d(I)$, ii) the interspike delay $d(I)$ is quantized with a USQ or the Lloyd quantizer (see Fig. 7 (b) iii) the reconstructed value \hat{I} is given by:

$$\hat{I} = \begin{cases} 0, & \text{if } \hat{d} > T, \\ h^{-1}(\hat{d}), & \text{otherwise,} \end{cases} \quad (38)$$

where $h^{-1}(\cdot)$ is defined in (21). The third quantization is given by the Dual-SIMQ (see Fig. 7 (c)).

The first goal of this section is to show that, in terms of compression, counting the number of spikes is more efficient than quantizing the delays (see Fig. 7 (c) and (b)). The second mission is to compare the proposed neuro-inspired quantizer with the state-of-the-art USQ and Lloyd quantizer when applied directly to the pixel intensities (see Fig. 7 (c) and (a)). Let the input intensities I_1, \dots, I_n correspond to the pixel values of each input image $I = (I_1, \dots, I_n)$. The quality evaluation of the results was measured by the Peak Signal-to-Noise Ratio (PSNR) metric (39) while the rate was computed according to (13). Throughout this paper the entropy is given in bits per pixel (bpp).

$$\text{PSNR}(I, \hat{I}) = 10 * \log_{10} \left(\frac{255^2}{\text{MSE}(I, \hat{I})} \right), \quad (39)$$

where $\text{MSE}(I, \hat{I})$ is defined by (10).



(a) Dual-SIMQ
 $\theta = 420 \text{ V}$
 PSNR = 46.05 dB
 $r = 5.43 \text{ bpp}$



(b) Dual-SIMQ
 $\theta = 5200 \text{ V}$
 PSNR = 23.75 dB
 $r = 1.93 \text{ bpp}$



(c) USQ
 $\theta = 420 \text{ V}, q = 0.01$
 PSNR = 44.43 dB
 $r = 5.45 \text{ bpp}$



(d) USQ
 $\theta = 5200 \text{ V}, q = 0.01$
 PSNR = 23.60 dB
 $r = 1.94 \text{ bpp}$



(e) LQ
 $\theta = 420 \text{ V}$
 PSNR = 43.63 dB
 $r = 5.4 \text{ bpp}$



(f) LQ
 $\theta = 5200 \text{ V}$
 PSNR = 26.96 dB
 $r = 2 \text{ bpp}$

Fig. 8: Visual comparison of the Dual-SIMQ (a)-(b), the USQ applied to the delays (c)-(d) and the Lloyd applied to the delays (e)-(f) for similar rates (set of parameters: $R = 10^3 \Omega$, $C = 1 \text{ F}$, $T = 100 \text{ ms}$).

Figure 8 visually compares the performance of the three quantization methods. As expected, the Dual-SIMQ is substantially better than the state-of-the-art USQ and LQ applied



(a) Dual-SIMQ
 $\theta = 310 \text{ V}$
 PSNR = 49.13 dB
 $r = 5.43 \text{ bpp}$



(b) Dual-SIMQ
 $\theta = 4200 \text{ V}$
 PSNR = 25.14 dB
 $r = 1.99 \text{ bpp}$



(c) USQ
 PSNR = 49.6 dB
 $r = 5.45 \text{ bpp}$



(d) USQ
 PSNR = 27.09 dB
 $r = 1.99 \text{ bpp}$



(e) LQ
 PSNR = 43.63 dB
 $r = 5.4 \text{ bpp}$



(f) LQ
 PSNR = 22.92 dB
 $r = 1.58 \text{ bpp}$

Fig. 9: Visual comparison of the Dual-SIMQ (a)-(b), the USQ applied to the pixels intensities (c)-(d) and the Lloyd applied to pixel intensities (e)-(f) for similar rates (set of parameters: $R = 10^3 \Omega$, $C = 1 \text{ F}$, $T = 100 \text{ ms}$).

to the delays. This is evident both numerically, by the fact that for similar rates the quality assessment using the Peak Signal-to-Noise Ratio (PSNR) metric (39) is higher, and visually especially for lower rates (see cases (b),(c) and (f)), where the details and the intensities range of the original image are better approximated by the neuro-inspired method. Figures 9 and 10 verify that for the same rate r (bpp) counting the number of spikes is more efficient than quantizing the pixel intensities either in a uniform or a non-uniform way. The experiment in

Fig. 10 exploits 100 natural images with $n = 256 \times 256$ pixels taken from the USC-SIPI database [31].

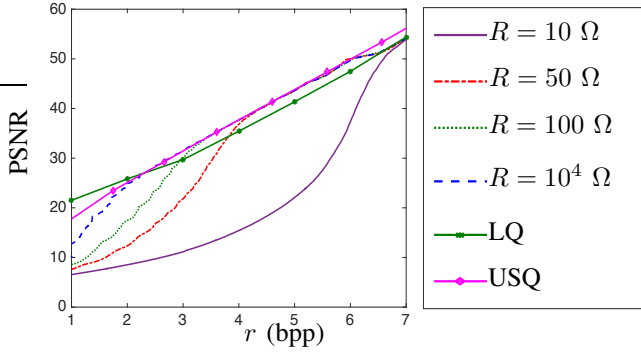


Fig. 10: Comparison between (i) the Dual-SIMQ, (ii) the USQ and (iii) the non-uniform Lloyd quantizer (set of parameters: $C = 1$ F, $T = 150$ ms, $\theta \in \{1, R, \dots, 10R\}$ V, $\lambda = q$, $q = \{1, 8, 10, 15, 20, 40, 60, 80, 100\}$).

C. Progressive Reconstruction

The Dual-SIMQ is a time-dependent quantizer as discussed in section IV-C. It is also evident according to Proposition 2 and Proposition 1 that the lengths of the quantization regions depend on T , especially the quantization step ℓ_∞ vanishes as T becomes arbitrarily large. Fig. 11 illustrates the dynamic behavior of the Dual-SIMQ comparing the reconstruction performance of the system for different observation windows T . As expected, when the available observation time of the Dual-SIMQ is short, the number of spikes that correspond to high intensities is limited. As a result, the quality of the reconstruction is poor because most of the small intensities will be represented by one or none spikes. On the other hand, when the observation window is large almost all the pixel intensities will manage to generate some spikes improving in that sense the reconstruction quality. As a consequence, the progressive enhancement of the reconstructed signal is definitely among the most important and ground-breaking benefits of the Dual-SIMQ taking under consideration that none of the state-of-the-art quantization methods is able to improve the quality of the signal along time.

VI. CONCLUSION

This paper has introduced a novel, bio-inspired encoder/decoder of natural images called the Dual-SIMQ. The Dual-SIMQ encoder is based on the LIF model, a very efficient spike generation mechanism which approximates the neural spiking process. The Dual-SIMQ decoder is a combination of two spike interpretation mechanisms which approximates the spike arrival delay by counting the number of spikes within a given observation window.

The Dual-SIMQ framework can play a pivotal role in the signal, image and video processing fields because it allows to encode the input values in a simple and dynamic manner, mimicking the neural behavior. At the same time, it enables to progressively reconstruct the input value, which seems very promising for video compression applications. The "bigger picture" of this work is the development of a new compression system that understands the visual word according to the

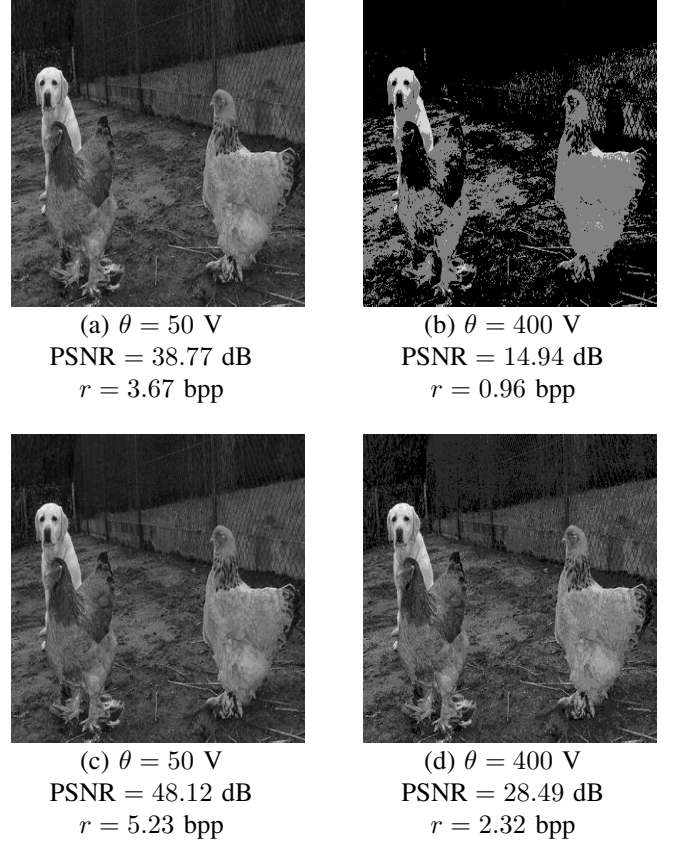


Fig. 11: Dual-SIMQ progressive reconstruction for $T = 50$ ms (a)-(b) and $T = 150$ ms (c)-(d) (set of parameters: $R = 10^3$ Ohm and $C = 1$ F).

human visual perception. Within this framework, merging different neuro-inspired processing tools, such as the retina-inspired filter [7] and the proposed Dual-SIMQ, could establish an alternative signal reconstruction methodology depending on neurons capabilities.

VII. ACKNOWLEDGEMENT

This work was partially funded by the Stavros Niarchos Foundation in the framework of the ARCHERS project.

APPENDIX A PROOF OF PROPOSITION 2

Let $f : [1, +\infty) \mapsto \mathbb{R}$ be the differentiable function:

$$f(x) = \frac{1}{1 - \exp\left(-\frac{\alpha}{x}\right)} \quad (40)$$

where $\alpha = T/\tau > 0$ and let $g(x) = f(x+1) - f(x)$. It is straightforward to verify that

$$\ell_k = \frac{\theta}{R} g(k), \forall k \geq 1.$$

Let us show that g is an increasing function. The first derivative of g is

$$g'(x) = f'(x+1) - f'(x) \quad (41)$$

where

$$f'(x) = \frac{\alpha \exp\left(-\frac{\alpha}{x}\right)}{x^2 \left(1 - \exp\left(-\frac{\alpha}{x}\right)\right)^2}. \quad (42)$$

A short calculation shows that

$$f'(x) = \frac{\alpha}{4x^2 \sinh^2\left(\frac{\alpha}{2x}\right)} \quad (43)$$

where $\sinh(\cdot)$ is the hyperbolic sine. Let $u : [1, +\infty) \mapsto \mathbb{R}$ be the function defined by

$$u(x) = x \sinh\left(\frac{\alpha}{2x}\right).$$

The function $u(x)$ is strictly decreasing over $[1, +\infty)$ since its first derivative is strictly negative. Indeed, we get

$$u'(x) = \sinh\left(\frac{\alpha}{2x}\right) - \frac{\alpha}{2x} \cosh\left(\frac{\alpha}{2x}\right)$$

where $\cosh(\cdot)$ is the hyperbolic cosine. So, $u'(x) < 0$ is equivalent to

$$\tanh\left(\frac{\alpha}{2x}\right) < \left(\frac{\alpha}{2x}\right).$$

A short calculation shows that

$$\tanh(y) < y, \forall y > 0,$$

where $\tanh(\cdot)$ is the hyperbolic tangent, which proves that $u'(x) < 0$ for all $x \geq 1$. Since $u(x)$ is strictly positive and strictly decreasing, $u^2(x)$ is also strictly decreasing. It follows that $f'(x)$ is strictly increasing. From (41), it follows that $g'(x) > 0$ for all $x \geq 1$. This shows that g is strictly increasing and, hence, ℓ_k is a strictly increasing sequence of reals.

Let us calculate the limit of the sequence ℓ_k . The Taylor series of $h^{-1}(x)$ at $x = 0$ is given by

$$h^{-1}(x) = \frac{\theta C}{x} + \frac{\theta}{2R} + \frac{\theta x}{12 R^2 C} + \frac{\theta}{R} o\left(\frac{x}{RC}\right), \quad (44)$$

where $o(\cdot)$ is the little-o notation such that $f = o(g)$ means that there exists a function $\varepsilon(x)$ satisfying $f = g\varepsilon$ and $\varepsilon(x) \rightarrow 0$ as $x \rightarrow 0$. Indeed, a short calculation shows that:

$$\frac{1}{1 - \exp(-x)} = \frac{1}{x} + \frac{1}{2} + \frac{1}{12}x + o(x), \quad (45)$$

and the derivation of (44) is straightforward. Assuming that k is large and applying (44) to each term of (29) yields

$$\ell_k = \frac{\theta C}{T} + o\left(\frac{1}{k}\right). \quad (46)$$

The limit ℓ_∞ is immediate.

Finally, let us show that $\ell_0 > \ell_\infty$. It is well known that $\exp(-x) > 1 - x$ for all $x \neq 0$. Hence, it follows that

$$\ell_0 = \frac{\lambda}{R} = \frac{\theta}{R} \left(1 - \exp\left(-\frac{T}{RC}\right)\right)^{-1} > \frac{\theta}{R} \frac{RC}{T} = \ell_\infty. \quad (47)$$

REFERENCES

- [1] W. Gerstner and W. Kistler, *Spiking neuron models: Single Neurons, Populations, Plasticity*, Cambridge University Press, 2002.
- [2] R. VanRullen and S. J. Thorpe, "Rate coding versus temporal order coding: what the retinal ganglion cells tell the visual cortex," *Neural Computation*, vol. 13, no. 6, pp. 1255–1283, 2001.
- [3] K. Masmoudi, M. Antonini, and P. Kornprobst, "Frames for exact inversion of the rank order coder," *IEEE Transactions on Neural Networks and Learning Systems*, vol. 23, no. 2, pp. 353–359, 2012.
- [4] A. A. Lazar and L. T. Tóth, "Perfect recovery and sensitivity analysis of time encoded bandlimited signals," *IEEE Transactions on Circuits and Systems I: Regular Papers*, vol. 51, no. 10, pp. 2060–2073, 2004.
- [5] Aurel A. Lazar, A. Pnevmatikakis, and Efthychios A. Pnevmatikakis, "Video Time Encoding Machines," *IEEE Transactions on Neural Networks*, vol. 22, no. 3, pp. 461–473, 2011.
- [6] Y. C. Yoon, "LIF and Simplified SRM Neurons Encode Signals into Spikes via a Form of Asynchronous Pulse Sigma-Delta Modulation," *IEEE Transactions on Neural Networks and Learning Systems*, vol. 28, no. 5, pp. 1192–1205, 2017.
- [7] E. Doutsis, L. Fillatre, M. Antonini, and J. Gaulmin, "Retina-inspired Filter," *IEEE Transactions on Image Processing*, vol. 27, no. 7, pp. 3484–3499, 2018.
- [8] Thomas Cover and Joy Thomas, *Elements of Information Theory*, John Wiley & Sons, Canada, second edition, 2006.
- [9] R. M. Gray and D. L. Neuhoff, "Quantization," *IEEE Transactions on Information Theory*, vol. 44, no. 6, pp. 2325–2384, 1998.
- [10] Bernard Widrow, Istvan Kollar, and Ming Chang Liu, "Statistical Theory of Quantization," *IEEE Transactions on Instrumentation and Measurement*, vol. 45, no. 2, pp. 353–361, 1996.
- [11] S. P. Lloyd, "Least Squares Quantization in PCM," *IEEE TRANSACTIONS ON INFORMATION THEORY*, vol. 28, no. 2, pp. 129–137, 1982.
- [12] C. Parisot, *Allocations Basées Modèles et transformée en ondelettes au fil de l'eau pour le codage d'images et de vidéos*, Ph.D. thesis, Université de Nice-Sophia Antipolis, 2003.
- [13] A. L. Hodgkin and A. F. Huxley, "Currents carried by sodium and potassium ions through the membrane of the giant axon of Loligo," *The Journal of Physiology*, vol. 116, no. 4, pp. 449–472, 1952.
- [14] R. FitzHugh, "Impulses and Physiological States in Theoretical Models of Nerve Membrane," *Biophysical Journal*, vol. 1, no. 6, pp. 445–466, 1961.
- [15] J. Nagumo, S. Arimoto, and S. Yoshizawa, "An Active Pulse Transmission Line Simulating Nerve Axon," *Proceedings of the IRE*, vol. 50, no. 10, pp. 2061–2070, 1962.
- [16] J. Rinzel, "Excitation dynamics: insights from simplified membrane models," *Theoretical Trends in Neuroscience: Federation proceedings*, vol. 44, no. 15, pp. 2944–2946, 1985.
- [17] J. Rinzel and G. B. Ermentrout, "Analysis of neural excitability and oscillations," *Methods in Neuronal Modeling*, pp. 251–292, 1989.
- [18] W. Gerstner, *A framework for spiking neuron models: The spike response model*, vol. 4, North-Holland, 2001.
- [19] L. F. Abbott and T. B. Kepler, *Model Neurons: from Hodgkin-Huxley to Hopfield*, Springer, Berlin, 1990.
- [20] E. D. Adrian, "The impulses produced by sensory nerve endings," vol. 61, no. 1, pp. 47–72, 1926.
- [21] David Heeger, "Poisson Model of Spike Generation," *Handout*, pp. 1–13, sep 2000.
- [22] S. J. Thorpe, D. Fize, and C. Marlot, "Speed of processing in the human visual system," 1996.
- [23] J. J. Hopfield, "Pattern recognition computation using action potential timing for stimulus representation," 1995.
- [24] Ole Jensen and John E. Lisman, "Hippocampal CA3 region predicts memory sequences: accounting for the phase precession of place cells," *Learning & memory (Cold Spring Harbor, N.Y.)*, vol. 3, no. 2-3, pp. 279–287, 1996.
- [25] Wolfgang Maass, "Lower Bounds for the Computational Power of Networks of Spiking Neurons," *Neural Computation*, vol. 8, no. 1, pp. 1–40, 1996.
- [26] John O'Keefe, "Hippocampus, theta, and spatial memory," *Current Opinion in Neurobiology*, vol. 3, no. 6, pp. 917–924, 1993.
- [27] S. J. Thorpe and M. Imbert, "Biological constraints on connectionist models," *Connectionism in perspective*, no. 63-92, 1989.
- [28] S. J. Thorpe, "Spike arrival times: A highly efficient coding scheme for neural networks," *R. Eckmiller, G. Hartmann & G. Hauske (Eds.), Parallel processing in neural systems and computers (pp. 91-94): North-Holland Elsevier*, 1990.
- [29] E. Doutsis, L. Fillatre, M. Antonini, and J. Gaulmin, "Bio-inspired Sparse Representation of Images," in *Groupe d'Etudes du Traitement du Signal et des Images (Gretsi)*, 2017.
- [30] E. Doutsis, L. Fillatre, M. Antonini, and J. Gaulmin, "Neuro-inspired Quantization," in *IEEE International Conference on Image Processing*, Athens, 2018.
- [31] A. Weber, "The USC-SIPI Image Database," 1977.